The 21st Conference of Mechanical Engineering Network of Thailand
17-19 October 2007, Chonburi, Thailand

Automated Detection of Singularities from Orientation Map of Isoclinics in Digital Photoelasticity

Pichet Pinit

Department of Mechanical Technology Education
Faculty of Industrial Technology Education and Technology
King Mongkut's University of Technology Thonburi
Bangmod, Toongkru, Bangkok 10140, Thailand
Tel: 0-2470-8526, E-mail: ipichet@yahoo.com

Abstract

In digital photoelasticity, the determination of the isoclinic parameter in its physical range is still the difficult problem. A recent work proposed by the author and his co-worker can effectively unwrap the orientation map regardless the existence of the singularities. The technique involves the detection of the singularities and the preservation of them for final processing with a certain limitation. That is, several regions that are not the singularities are detected. They can make the phase unwrapping algorithm taking more execution times. In this paper, a method for accurately detecting the positions of the singularities is proposed and evaluated with the orientation maps of the circular ring under compressive load obtained on the basis of the phase-shifting technique. Experimental results are also presented and discussed.

Keywords: Digital photoelasticity, Directional Map, Orientation Map, Phase-shifting technique, Singularities

1. Introduction

Photoelasticity is a powerful experimental technique which enables a complete stress analysis to be carried out on engineering structural components at the design stage. However, the analysis can be tedious process and is normally only carried out by an expert. At present day, the field of digital photoelasticity has been developed by integrating a new data acquisition and data processing to the conventional photoelasticity.

In digital photoelasticity, two fringe patterns, i.e., an isoclinic fringe pattern and an isochromatic fringe pattern, are given in the form of a digital image (an intensity data). These fringe patterns provide both magnitude and directions of stresses. The isoclinic fringe pattern enables the isoclinic parameter ϕ, which directly relates to the principal stress directions or directional map, to be determined whereas the isochromatic fringe pattern enables the isochromatic parameter δ, which directly relates to $(\sigma_1 - \sigma_2)$, to be evaluated.

For ϕ, a number of automated whole-field approaches have been proposed to determine it, particularly the whole-field method based on phase-shifting technique (PST) [1]. By PST, two problems arise when calculating ϕ, i.e., the isochromatic-isoclinic interaction [1] and wrapped phase map. The first problem occurs because of the unreliability of the isoclinic parameter at and near the isochromatic fringe skeleton. The wrapped phase data arises because only unambiguous phase is known at most in the range $(-\pi/4, +\pi/4]$* instead of $(-\pi/2, +\pi/2]$.

For the wrapped isoclinics, if it is left unsolved, the ambiguity exists on whether the map of isoclinics shows σ_1 or σ_2 directions over the entire domain. That this map of wrapped isoclinics can refer to both principal-stress directions leads to the name 'orientation map'.

To bring the isoclinic parameter ϕ to its physical range, the phase unwrapping (PU) is necessary. Recently, PU was proposed for unwrapping the map of wrapped isoclinics in which the singularities were taken in the consideration [2]. In that work, the crucial step is to detect the singularities and only one orientation map was used. The binary mask image representing the points detected shows some erroneous detected positions.

In this paper, the detection of such points based on the combination of the orientation maps is present. The detection technique is applied to the problem of circular ring under compression.

2. Computation of Principal-stress Directional Field

2.1 Theoretical aspect

The theoretical expression of the isoclinic parameter ϕ is well known as

$$\tan 2\phi = \frac{2\tau_{xy}}{\sigma_{xx} - \sigma_{yy}} \tag{1}$$

where σ_{xx}, σ_{yy} and τ_{xy} are the two-dimensional stress components in the Cartesian coordinates.

Then, for ϕ, inverting Equation (1) yields

$$\phi = \frac{1}{2}\arctan\left(\frac{2\tau_{xy}}{\sigma_{xx} - \sigma_{yy}}\right) \tag{2}$$

* $(a, b]$ represents $a < x \le b$ in which x is a variable of interest.

Table 1. Formation of the singularities according to the different values of the Cartesian stress components in Equation (2) [4]

Stress condition	Singularity
$\sigma_{xx} = \sigma_{yy} \neq 0$ and $\tau_{xy} = 0$	isotropic point
$\sigma_{xx} = \sigma_{yy} = 0$ and $\tau_{xy} = 0$	singular point
$\sigma_{xx} = \sigma_{yy} = \infty$ and $\tau_{xy} = \infty$	pole

Equation (2) provides $\phi \in (-\pi/4, +\pi/4]$ by using the ordinary arctangent operation. It should be noted here that even though Equation (1) is theoretically derived, the ambiguity always exists unless PU is applied.

2.2 Experimental aspect based on photoelasticity

An equation of the intensity I for different angular positions θ at the steps m of the dark-field plane polariscope with the white light source (Figure 1) can be expressed as [1]

$$I_{m,\lambda} = I_{\mathrm{mod},\lambda} \sin^2 2(\phi - \theta) + I_{\mathrm{b},\lambda} \tag{3}$$

where

$$I_{\mathrm{mod},\lambda} = \frac{1}{\Delta\lambda} \int_{\lambda_1}^{\lambda_2} I_{\mathrm{p},\lambda} \sin^2(\pi N_\lambda)\, d\lambda \tag{4}$$

λ (= R, G, B) is the primary wavelengths of the white light source, $\Delta\lambda = \lambda_2 - \lambda_1$ in which λ_2 and λ_1 are the upper and lower limits of the spectrum of the light, $I_{\mathrm{p},\lambda}$ is the light coming out of the polarizer, N_λ (= δ_λ / 2π) is the relative fringe order and $I_{\mathrm{b},\lambda}$ is the background intensity.

The expression for the orientation field of isoclinics based on the application of the four-step phase shift method to Equation (3) for m = 1, 2, 3, and 4 can be written as [2, 3]

$$\phi_{\mathrm{w}} = \frac{\pi}{8} - \frac{1}{4} \arctan\left(\frac{I_1^{\mathrm{s}} - I_3^{\mathrm{s}}}{I_2^{\mathrm{s}} - I_4^{\mathrm{s}}} \right) \quad \text{for} \quad I_{\mathrm{mod}}^{\mathrm{s}} \neq 0 \tag{5}$$

where

$$I_m^{\mathrm{s}} = \sum_\lambda I_{m,\lambda} = I_{m,\mathrm{R}} + I_{m,\mathrm{G}} + I_{m,\mathrm{B}} \tag{6}$$

$$\begin{aligned} I_{\mathrm{mod}}^{\mathrm{s}} &= I_{\mathrm{mod,R}} + I_{\mathrm{mod,G}} + I_{\mathrm{mod,B}} \\ &= \sqrt{(I_1^{\mathrm{s}} - I_3^{\mathrm{s}})^2 + (I_2^{\mathrm{s}} - I_4^{\mathrm{s}})^2} \end{aligned} \tag{7}$$

The subscript 'w' denotes that ϕ is of wrapped isoclinics of the range $(0, +\pi/4]$ due to the use of the ordinary arctangent operation.

3. Definition of Singularities

The singularities are one of the properties of the orientation or the directional field of isoclinics in which the state of stresses satisfies certain conditions. The following well-known theoretical formula will help in an explanation of the formation of the singularities.

$$\sigma_1, \sigma_2 = \frac{\sigma_{xx} + \sigma_{yy}}{2} \pm \frac{1}{2} \sqrt{(\sigma_{xx} - \sigma_{yy})^2 + 4\tau_{xy}^2} \tag{8}$$

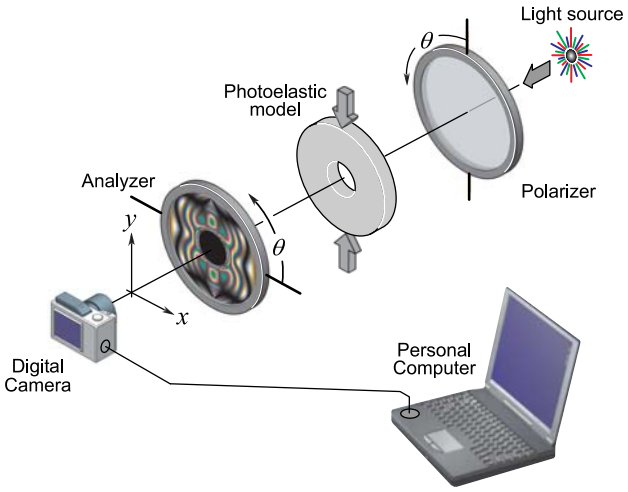

Figure 1. Dark-field plane polariscope system with the white light source having the circular ring model being placed inside and vertically loaded by a force.

As seen in Equation (2), there are three cases that cause the formation of the singularities in such orientation or directional field of the isoclinics. Table 1 lists all these three cases.

4. Modulated Intensity

As seen in Equation (4), $I_{\mathrm{mod},\lambda}$ is the function of the wavelength λ and the fringe order N_λ by which the relation between the fringe order and the principal-stress difference is expressed as [1]

$$N_\lambda = \frac{\delta_\lambda}{2\pi} = \frac{h}{f_{\sigma,\lambda}} (\sigma_1 - \sigma_2) \tag{10}$$

where h is the thickness of the model studied and $f_{\sigma,\lambda}$ is the well-known material stress fringe value obtained by calibration at wavelength λ.

Since, at the isotropic point and the singular point, $(\sigma_1 - \sigma_2) = 0$, then, at such points $N_\lambda = I_{\mathrm{mod},\lambda} = I_{\mathrm{mod}}^{\mathrm{s}} = 0$ (see Equations. (4) and (10)). This is the condition of the zeroth-order fringe. Then, the isotropic point and the singular point are seen as dark spots or regions in the map of the modulated intensity regardless the wavelengths used. By this fact, $I_{\mathrm{mod}}^{\mathrm{s}}$ can be used to detect such points.

It is worthy to note that when dealing with the real data, the condition may not give the correct positions because, at such points, the intensity may not be exact zero. As a result, it is possible to apply a tolerance to cope with this situation.

Then, if the values of $I_{\mathrm{mod}}^{\mathrm{s}}$ at any point or pixel in the map of the modulated intensity is equal or less than that of $T_{\mathrm{mod}}\, I_{\mathrm{mod,max}}^{\mathrm{s}}$, where T_{mod} is a predefined threshold or tolerance having values between 0.1 to 0.2 and $I_{\mathrm{mod,max}}^{\mathrm{s}}$ is the maximum value of the map of $I_{\mathrm{mod}}^{\mathrm{s}}$, such pixel is considered to be the singularities, especially the isotropic and singular points.

5. Method of Detection of Singularities

The method for the detection of the singularities is as followings.

- Detection of the singularity-to-be pixels: this is done by performing a raster scan over the orientation maps of the ranges [0, +π/2] and (−π/4, +π/4] using a mask window $w^{d}_{m\times n}$ and over the map of modulated intensity with the condition $T_{\text{mod}}\, I^{s}_{\text{mod,max}}$. In case of the scanning over the orientation maps, if the distribution of the isoclinics around any pixel is similar to the standard distribution that pixel is selected [2,4]. The standard distribution of the isoclinics depends on the abrupt jumps of the isoclinics around the pixel which directly relate to the type of the singularities; that is, for the positive type of singularities the isoclinic values vary around such pixel counterclockwise whereas for the negative type of singularities the isoclinic values vary around such pixel clockwise [5]. Also, for the scanning over the map of the modulated intensity, any pixel satisfying the condition mentioned above is chosen. The pixels detected are separately stored into three binary arrays, i.e., $A_{[0,\,+\pi/2]}$, $A_{(-\pi/4,\,+\pi/4]}$ and A_{mod}, respectively. Note that these arrays are initially populated with one value. For the pixels found as the tentative singularities in those maps of the isoclinic orientation and the modulated intensity, the corresponding pixels in the associated arrays are reset to zero value.

- Selection of the singularities: since, in all those three arrays, the pixels representing the positions of the singularities have the zero value, then, for clarity, let the parameters α, β, and γ respectively be the values of the pixels in the arrays $A_{[0,\,+\pi/2]}$, $A_{(-\pi/4,\,+\pi/4]}$ and A_{mod}. Also, let A_{sin} be another binary array used for storing final results. This array is initially populated with one value. Two following operations are of interest and they are:

  (1) Doublet function $D(\alpha, \beta)$: for the same position of the two pixels in both binary arrays $A_{[0,\,+\pi/2]}$ and $A_{(-\pi/4,\,+\pi/4]}$, if $D(\alpha, \beta) = D(0, 0)$, the pixel at that position in the array A_{sin} is then assigned to be the singularities by setting it to zero value.

  (2) Triplet function $T(\alpha, \beta, \gamma)$: for the same position of the three pixels in the three binary arrays $A_{[0,\,+\pi/2]}$, $A_{(-\pi/4,\,+\pi/4]}$, and A_{mod}, if $T(\alpha, \beta, \gamma) = T(0, 0, 0)$, the pixel at that position in the array A_{sin} is then assigned to be the singularities by setting it to zero value.

  Note that the raster scan for performing the doublet and/or triplet functions can be simply done pixel-by-pixel over those the binary arrays.

6. Results and Discussion

The dark-field plane polariscope system used is the same as that already reported [2] and it is graphically shown in Figure 1. To examine the method proposed here, it was applied to the problem of the circular ring under the vertically diametral compression. The model was made of 6-mm thick epoxy resin plate with 10-mm inner and 30-mm outer diameters.

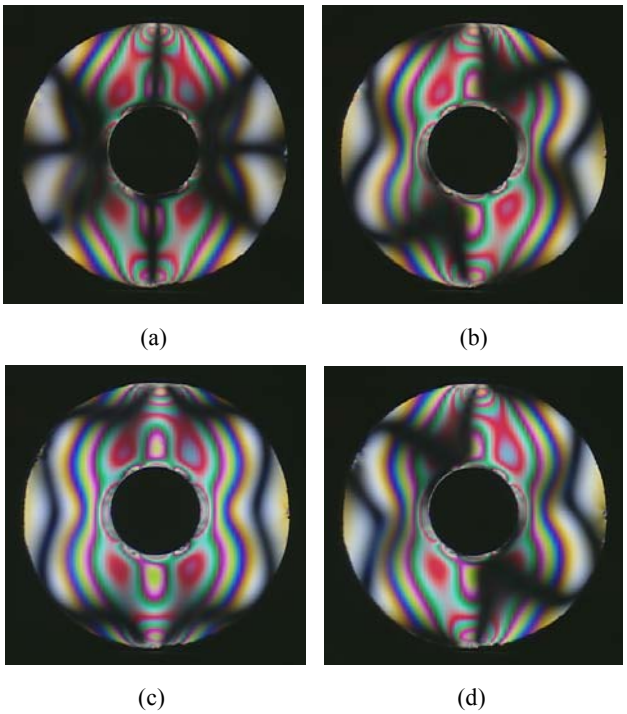

(a) (b) (c) (d)

Figure 2. Experimentally generated color photoelastic fringe images of circular ring for four different angular configurations of the crossed polarizer and analyzer. (a) $\theta = 0$, (b) $\theta = +\pi/8$, (c) $\theta = +\pi/4$, and (d) $\theta = +3\pi/8$. (Printed in black and white.)

Once the model was properly placed in the polariscope system and loaded by a force P of 274 N, the four photoelastic fringe images were digitally collected for the four different dark-field configurations of the plane polariscope. Figure 2 shows these photoelastic fringe images. These images are the same as those used in the previous work [2]. The digital camera used for the collection of the color photoelastic fringe images was of Nikon model D70.

Figure 3(a) shows the resultant map obtained after applying Equation (5) to Figure 2 with the normalization [2, 3]. It should be noted that this orientation map shows $\phi_w \in [0, +\pi/4]$. Figures 3(b) and (c) report the orientation maps of the range [0, +π/2] and (−π/4, +π/4], respectively. They were obtained from Figure 3(a) using the simple logic operations [2]. Figure 3(d) displays the map of I^{s}_{mod}. It should be noted here that this model contains two isotropic points and eight singular points [5].

Close scrutiny of Figures 3(a)-(c) reveals that the lines representing the abrupt isoclinic jumps are not smooth as they should be. This because the isochromatic-isoclinic interaction. That is, Equation (5) is theoretically invalid when $I^{s}_{\text{mod}} = 0$; however, for the experimental data, the true condition is $I^{s}_{\text{mod}} \approx 0$. Hence, the closer are the values of I^{s}_{mod} to zero; the more obvious is the effect of the isochromatics on the maps of the isoclinics.

Comparing Figures 3(a)-(d) to (e) reveals that the

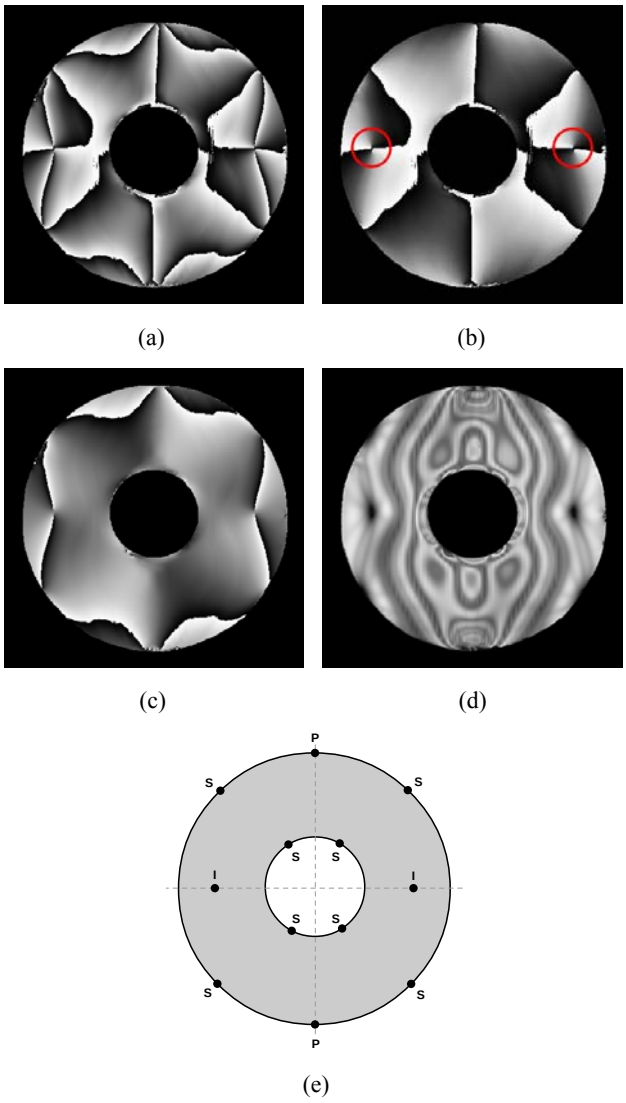

Figure 3. Orientation maps and Modulated intensity map. (a) orientation map of the range (0, +π/4], (b) orientation map of the range [0, +π/2], (c) orientation map of the range (−π/4, +π/4], (d) modulation map and (e) position of the singularity. 'I', 'S' and 'P' label the isotropic points, singular points and poles, respectively. The values of the modulated intensity and of isoclinics are separately and linearly converted into the 256-gray levels where 0 represents deep black and 255 represents pure white.

positions of the isotropic points, singular points and poles are clearly observed, particularly, the isotropic points (see circles in Figure 3(b)). However, the four singular points lying on the inner boundary are rather vague.

The other four singular points lying on the outer boundary are seen since the lines representing the abrupt isoclinic jumps pass through them (Figures 3(a)-(c)). Their positions can be also observed in Figure 3(d) as the dark regions making the outer boundary incomplete.

Figure 4 shows the binary images representing the positions of the singularities. Figure 4(a) was the result of the raster scan over Figure 3(b) whereas Figure 4(b) was

Table 2. Values of parameters used in the detection of the singularities [2]

Parameter	Value
T_{mod}	0.1
Detecting mask window, $\mathrm{w}^{\mathrm{d}}_{m\times n}$	$\mathrm{w}^{\mathrm{d}}_{21\times 21}$

obtained by performing the raster scan over Figure 3(c). Figure 4(c) shows the map of the singularities found by the condition $T_{\mathrm{mod}}\, I^{\mathrm{s}}_{\mathrm{mod,max}}$. These maps were obtained using the parameters listed in Table 2. Figures 4(d) and (e) report the results obtained by the functions $D(\alpha, \beta)$ and $T(\alpha, \beta, \gamma)$, respectively.

Observation of Figures 4(a) and (b) reveals that the isotropic points and poles were correctly detected. This can be confirmed by considering Figure 4(c). However, there are other detected positions that are not of the singularities (see circles in Figure 4(a)). As seen, these erroneous regions do not appear in Figure 4(b) since the isoclinics around the regions are smoothly continuous (see Figure 3(c)).

After completely performing the doublet function, the erroneous regions were totally discarded whereas as for the triplet function, the map shows only the isotropic points and small dark region at the bottom of Figure 4(e). It should be noted that at the poles, $(\sigma_1 - \sigma_2)$ approaches $+\infty$; therefore, such small dark region appeared in Figure 4(e) is not the result of the condition $T_{\mathrm{mod}}\, I^{\mathrm{s}}_{\mathrm{mod,max}}$. However, due to the applied load, the geometrical shape of the model at the poles may be slightly deformed and this effect makes a variation in the values of $I^{\mathrm{s}}_{\mathrm{mod}}$. As a result, some values of $I^{\mathrm{s}}_{\mathrm{mod}}$ may be lower than such condition and then it was found as the singularities (considering the bottom portion of Figure 4(c)). It is informative noting that the poles can be only detected by using the abrupt isoclinic jumps around them (Figures 4(a) and (b)).

For the use of $T_{\mathrm{mod}}\, I^{\mathrm{s}}_{\mathrm{mod,max}}$, the isotropic points were accurately detected as the two dark regions in Figure 4(c). Nevertheless, the position of the singular points are not clear but they can be seen if one makes a scrutiny on Figure 4(c) and compare to Figure 3(d) for the dark regions lying on the outer boundary.

Figure 4(f) shows the unwrapped phase map of the isoclinics shown in the physical range (−π/2, +π/2]. This map of unwrapped isoclinics was obtained from proposed PU algorithm [2] combined with the method proposed here. As seen, the directional field around the isotropic points is correct. It is worthy to note the difference between the orientation maps (Figs. 3(a)-(c)) and the directional map (Fig. 4(f))

7. Conclusions

In this paper, the automated technique for detection of the singularities has been presented. The technique involves the use of the two orientation maps of the ranges [0, +π/2] and (−π/4, +π/4] and the map of modulated intensity $I^{\mathrm{s}}_{\mathrm{mod}}$. Results of the binary images show that the isotropic points can be correctly found using the triplet

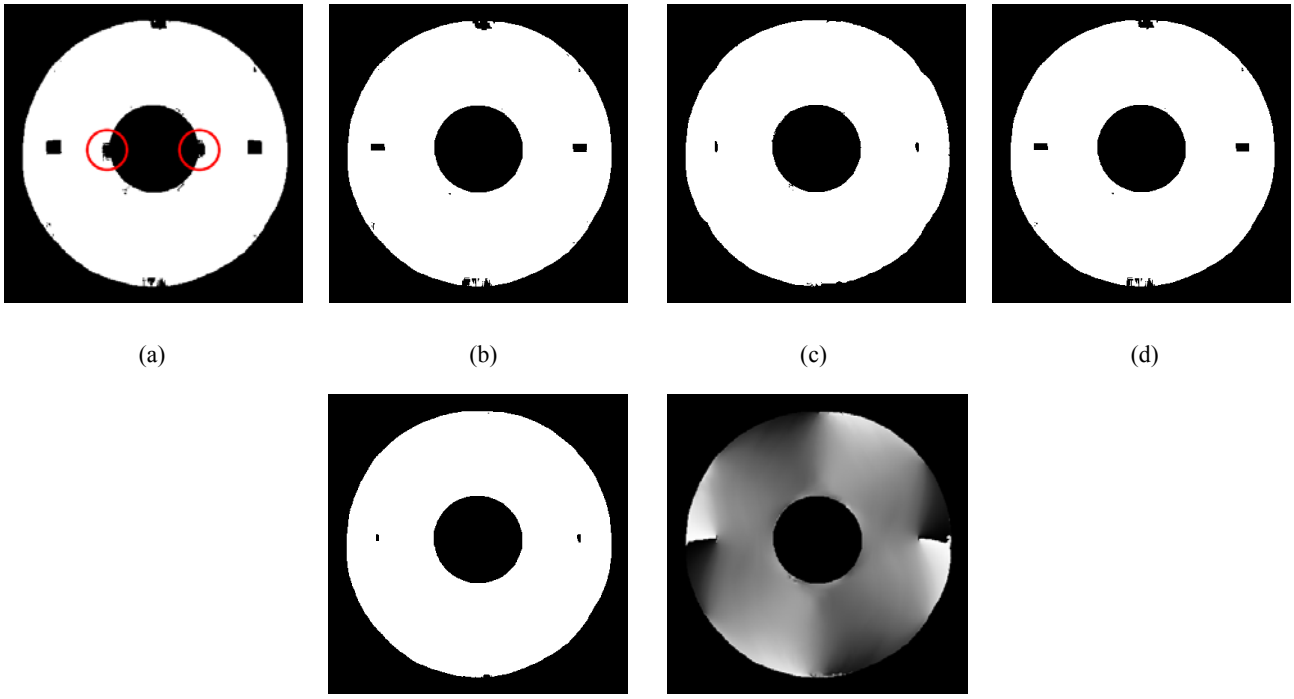

Figure 4. Binary images representing the position of the singularities obtained from (a) $A_{[0,+\pi/2]}$, (b) $A_{(-\pi/4,+\pi/4]}$, (c) A_{mod}, (d) A_{sin} by $D(\alpha, \beta)$, (e) A_{sin} by $T(\alpha, \beta, \gamma)$ and (f) directional map of the range $(-\pi/2, +\pi/2]$ by which black represents $-\pi/2$ and white represents $+\pi/2$.

function whereas the isotropic points, singular points and the poles are totally detected by the doublet function.

Due to the mechanical stable at the isotropic points and the singular points, this would give a practical benefit for the optimum design of the structural members with fasteners (Figures 4(c) and (e)). However, in the view of PU, the directional map obtained only using the doublet function is good for the requirements of PU algorithm [2]. That is, as seen in Figure 4(d), the isotropic points, singular points and pole are found. Since they can cause failure of PU, totally finding them makes PU more stable.

It is seen that Figure 4(b) can also be used in PU as in the case Figure 4(d) because they look similar. However, this similarity may not happen for the other models; therefore, the use of the binary image obtained from the doublet function is more appropriate.

It is informative to note that with the map of unwrapped isoclinics or the directional map the isostatics or the lines of the principal stress directions can be directly obtained. The isostatics is very useful for the optimum shape design of the structural members.

References

[1] Ramesh, K., 2000. Digital Photoelasticity: Advanced Techniques and Applications. Springer, New York.

[2] Pinit, P., and Umezaki, E., 2007. Digitally whole-field analysis of isoclinic parameter in photoelasticity by four-step color phase-shifting technique. Optics and Lasers in Engineering, Vol. 45, No. 7, pp. 795-807.

[3] Pinit, P. and Umezaki, E., 2005. Full-field determination of principal-stress directions using photoelasticity with plane polarized RGB lights, Optical Review, Vol. 12, No. 3, pp. 228-232.

[4] Umezaki, E., Waranabe, H., Sirichai, S. and Shimamoto, A., 1994. Extraction of singular points from photoelastic measurement, *Recent Advances in Experimental Mechanics* (Gomes, S., et al., eds.), Rotterdam, Netherlands, pp. 107-112.

[5] Frocht, M.M., 1948. Photoelasticity, Vol. 1, John Willey & Sons, New York.